ACS OMEGA

Open Access

http://pubs.acs.org/journal/acsodf

Article

Reduced Surface Trap States of PbS Quantum Dots by Acetonitrile Treatment for Efficient SnO_2-Based PbS Quantum Dot Solar Cells

Guannan Xiao,* Taohua Liang, Xiaoming Wang, Chao Ying, Kai Lv, and Chengwu Shi*

Cite This: *ACS Omega* 2024, 9, 12211−12218

Read Online

ACCESS | Metrics & More | Article Recommendations | Supporting Information

ABSTRACT: The solution-phase ligand-exchange strategy offers a simple pathway to prepare PbS quantum dots (QDs) and their corresponding solar cells. However, the production of high-quality PbS QDs with reduced surface trap state density for efficient PbS QD solar cells (QDSCs) still faces challenges. As the hydroxyl group (−OH) has been demonstrated to be the primary source of the surface trap states on PbS QDs in the general oleic acid method, here, we present an effective and facile strategy for reducing the surface −OH content of PbS QDs by using acetonitrile (ACN) as precipitant to wash the surface of QDs, which significantly decreases the trap state density and enables the preparation of superior PbS QDs. The resulting solar cell with an ITO/SnO_2/n-PbS/p-PbS/Au structure obtained an improved photoelectric conversion efficiency (PCE) from 8.53 to 10.49% with an enhanced air storage stability, realizing a high PCE for SnO_2-based PbS QDSCs.

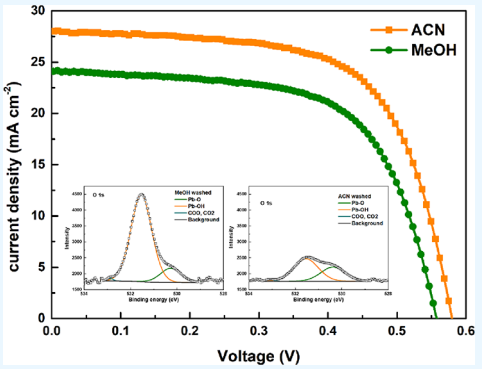

1. INTRODUCTION

As optoelectronic materials with great research potential and application prospect, PbS quantum dots (QDs), with their low synthesis cost, tunable band gap, multiple exciton generation, and large exciton Bohr radius of 18 nm, possess a broad range of applications in photovoltaics including photodetectors, light-emitting diodes, and photovoltaic devices.[1−7] Their photoelectric properties can be widely adjusted through size control and surface chemical modification to meet the design requirements of various functions and properties.[8,9] For QDSCs, with the improvement of QD synthesis, surface passivation, and solar cell structure, the photoelectric conversion efficiency (PCE) has improved rapidly,[10−14] and the highest certified PCE of PbS QDSC has exceeded 13% so far.[15] On the other hand, the large trap state density on the surface of PbS QD films seriously affects the photovoltaic performance of PbS QDSCs. Recent studies on PbS QDs have shown that for the oleate-capped PbS (o-PbS) QDs using PbO and oleic acid (OA) ligand, the nonpolar (001) surfaces can be passivated by the covalent bond of the carboxyl group (−COOH), whereas the polar (111) surfaces of Pb terminal are passivated by the deprotonated carboxyl group (COO^-) and hydroxyl group (−OH), in which the −OH is regarded as the main cause of surface trap states on PbS QDs.[16−18] There have been various reported strategies to reduce the −OH content, promising further improvement in the photovoltaic performance and stability of PbS QDSCs. Jang et al.[17] prepared surface trap-passivated PbS QDs by using PDMII instead of TBAI as iodide source for ligand exchange, which effectively removed the −OH on the PbS QD surface. The resulting PbS QDSCs with the structure of ITO/ZnO/n-PbS/p-PbS/Au obtained a certified PCE of 10.89%. Konstantatos et al.[18] successfully suppressed the −OH on the PbS QD surface through thermal annealing of QD layers at 80 °C and by using EMII instead of TBAI for ligand exchange, and the corresponding PbS QDSCs with the structure of ITO/ZnO/n-PbS/p-PbS/Au had a PCE of 9.6%. Therefore, developing a new strategy to reduce the −OH content on the surface of PbS QDs is an important approach to improve the photovoltaic performance and stability of PbS QDSCs. On the other hand, it is worth noting that most PbS QDSCs with high photovoltaic performance use ZnO or TiO_2 thin film as the electron transporting layer (ETL), and there are currently limited reports on the application of SnO_2 as the ETL in PbS QDSCs. Compared with ZnO and TiO_2, SnO_2 possesses high electron mobility, wide band gap, and good light transmittance.[19−22] Song et al.[23] assembled PbS QDSCs by using SnO_2-Cl as the ETL, and the corresponding solar cells obtained a PCE of 9.37%. Ma et al.[24] prepared a SnO_2 thin film by magnetron sputtering and combined it with a 10 nm thick ZnO thin film to form a double-layer electron transporting layer. The corresponding PbS QDSC reached a PCE of 10.1%. Consequently, studies on the application of SnO_2 in PbS QDSCs have great development potential and research significance.

Received: January 7, 2024
Revised: February 1, 2024
Accepted: February 22, 2024
Published: February 29, 2024

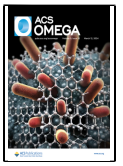

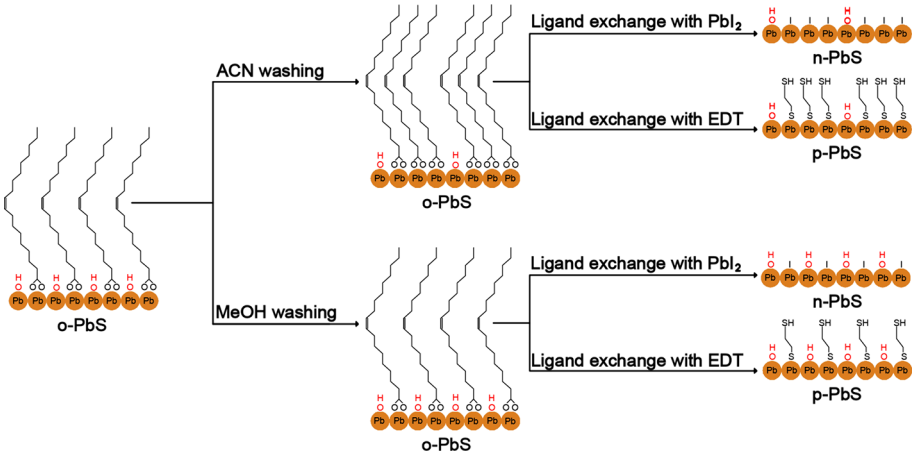

Figure 1. Schematic illustration of the PbS QD surface washed by ACN and MeOH.

Herein, we prepared a surface-passivated SnO_2 thin film as the ETL for assembling PbS QDSCs. And for the first time, we present an effective and facile strategy for reducing the surface −OH content of PbS QDs by using ACN as precipitant to wash the surface of QDs, which is quite different from the previous work that usually applied different kinds of halide salts to reduce the surface −OH of PbS QDs. The resulting PbS QDs exhibited a significantly reduced surface −OH content, which effectively decreased the surface trap states and suppressed the charge recombination. The influence of different precipitants on surface trap states of PbS QDs and the photovoltaic performance of PbS QDSCs were systematically investigated. The corresponding PbS QDSC based on ACN-washed PbS QDs and SnO_2 ETL achieved a PCE of 10.49% with high air storage stability, which was a high level of PCE for SnO_2 ETL based PbS QDSCs.

2. EXPERIMENTAL SECTION

2.1. Synthesis of PbS QDs with Reduced Surface Trap States. PbS QDs were synthesized via a solution-phase ligand-exchange process with some modification.[11,25,26] In this work, the hexamethyldisilathiane (TMS)/1-octadecene (ODE) mixture was obtained by adding 210 μL of TMS into 8 mL of the ODE that had been degassed at 80 °C for 12 h in advance. Pb-oleate was obtained by dissolving 0.45 g of PbO, 1.5 mL of OA, and 18 mL of ODE into a 50 mL three-neck flask and stirred at 95 °C for 2 h in a vacuum state. After that, a steady N_2 flow was introduced into the flask to keep a N_2 atmosphere. Then the prepared TMS/ODE mixture was injected into the Pb-oleate at 125 °C. The resulting mixture was centrifuged at 5000 rpm for 5 min after adding 50 mL of acetone and naturally cooling down to room temperature. After 8 mL of ACN was added, the precipitate of the mixture was dispersed in 4 mL of toluene followed by another centrifugation at 8500 rpm for 10 min. The obtained precipitates of PbS QDs were dispersed in 6 mL of octane and kept in reserve with a N_2 atmosphere.

The PbI_2 mixed solution was obtained by dissolving 0.031 g of CH_3COONH_4, 0.461 g of PbI_2, and 0.073 g of $PbBr_2$ into 10 mL of dimethylformamide (DMF) solution. The 4 mL of obtained PbS QD octane solution was diluted to 10 mL by octane and then mixed vigorously with the PbI_2 mixed solution for 3 min. Triple washings with octane were then performed on the resulting PbS QDs in DMF phase, which were precipitated after mixing with 5 mL of toluene. After being centrifuged, the PbS QDs were dried by a constant N_2 flow to obtain QD powder. The n-PbS QDs were prepared by dispersing the dried PbS QDs in 0.8 mL of butylamine, and the p-PbS QDs were obtained by filtering the remaining 2 mL of obtained PbS QD octane solution.

2.2. Device Fabrication. On the cleaned indium-doped tin oxide (ITO) substrate, the 1.5 wt % SnO_2 solution was spin-coated at 3000 rpm for 30 s and then air-annealed at 150 °C for 30 min to obtain the SnO_2 film. The passivated SnO_2 electron transporting layer was prepared by spin-coating at 3000 rpm for 30 s with a 0.05 M $SnCl_2$ ethanol solution on the SnO_2 film followed by successive annealing at 100 °C for 30 min and 180 °C for 60 min, respectively.[27] For the n-PbS film, 90 μL of n-PbS QDs was spin-coated on the passivated SnO_2 electron transporting layer at 2500 rpm for 30 s. For the p-PbS film, 80 μL of p-PbS QDs was spin-coated on the n-PbS film at 2500 rpm for 30 s followed by the 1,2-ethanedithiol (EDT, 0.04 vol % in ACN) and ACN rinsing twice. The gold electrode was then deposited on the p-PbS film with a thickness of 80 nm. The structures of the PbS QDSCs were ITO/SnO_2/n-PbS/p-PbS/Au.

2.3. Characterization and Measurement. The size of the PbS quantum dots was observed by transmission electron microscopy (FEI F20 FEG-STEM). The surface −OH content of PbS QDs was measured by X-ray photoelectron spectroscopy (XPS, Kratos Ultra). The space charge-limited current (SCLC) $I-V$ measurements were applied on the devices with the structure of ITO/SnO_2/n-PbS/BCP/C_{60}/Ag for the electron-only device and the structure of ITO/PEDOT:PSS/p-PbS/*spiro*-OMeTAD/Au for the hole-only device. An Ivium-n-Stat was then used to measure the current under dark conditions with applied voltages, and the nonlinear response was analyzed based on the SCLC theory.[28] $C-V$ characterization was performed by an Ivium-n-Stat under dark conditions with a voltage amplitude of 10 mV at a frequency of 1 kHz. Electrochemical impedance spectra (EIS) were collected by an electrochemical workstation under dark conditions, with frequencies from 1 to 1×10^6 Hz, and the Nyquist plot was obtained by fitting the measured data using the EC-lab software according to the corresponding equivalent circuit. The photocurrent−photovoltage characteristics of solar cells with an active area of 0.08 cm^2 were characterized under a solar simulator (Newport, Oriel Class AAA, 94063A) at 100 $mW \cdot cm^{-2}$ illumination (AM 1.5 G) calibrated by an NREL-certificated silicon reference cell (Newport, 91150 V).

https://doi.org/10.1021/acsomega.4c00208
ACS Omega 2024, 9, 12211−12218

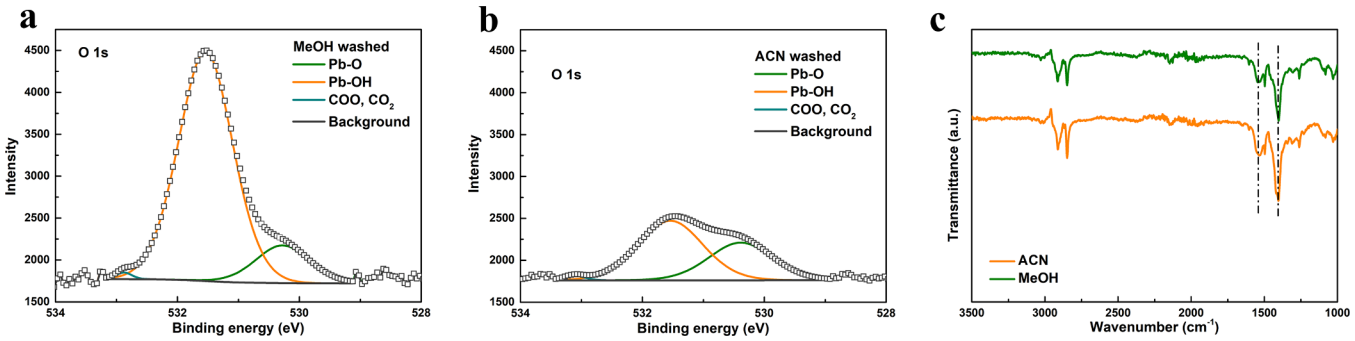

Figure 2. O 1s XPS spectra of o-PbS QDs washed with (a) MeOH and (b) ACN. (c) FTIR spectrum of ACN-washed and MeOH-washed oleate-capped PbS QDs.

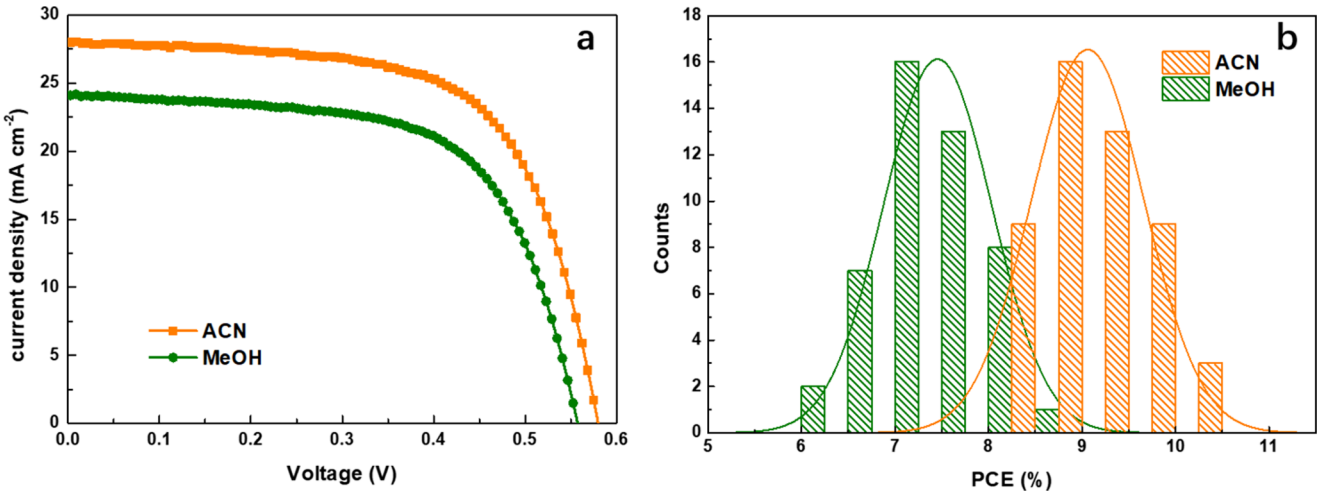

Figure 3. (a) Photocurrent−photovoltage characteristics of ACN-washed and MeOH-washed PbS QDSCs. (b) Statistics of the PCE distribution of ACN-washed and MeOH-washed PbS QDSCs.

3. RESULTS AND DISCUSSION

3.1. Influence of Different Precipitants on the Surface −OH of PbS QDs. As one of the main sources of surface trap states, the hydroxyl group on the (111) surface facets had a negative impact on the photovoltaic performance and stability of PbS QDSCs. Therefore, as shown in Figure 1, to decrease the surface trap states of PbS QDs and further improve the quality of n-type PbS (n-PbS) and p-type PbS (p-PbS), we developed a simple but effective strategy based on previous reports of PbS QDs synthesis using ACN instead of the traditional precipitant methanol (MeOH) to wash the surface of PbS QDs.[11,25] The −OH on the PbS QDs surface was indicated by the O 1s peaks from XPS analysis, and the results were shown in Figure 2. According to previous reports, the peaks at 532.9, 530.3, and 531.5 eV can be corresponding to the characteristic peaks of $-COO^-$ or CO_2, Pb−O, and Pb−OH, respectively.[16,17,29,30] It can be clearly observed that the peak located at 531.5 eV showed less than one-third intensity in the ACN washed o-PbS compared to MeOH washed o-PbS, indicating that the content of −OH on the PbS QDs surface had a dramatic decrease by using ACN to wash PbS QDs. As shown in Figure 2c, Fourier transform infrared spectroscopy (FTIR) analysis has been added to further identify the surface chemistry of ACN-washed and MeOH-washed QDs. The peaks at around 1400 and 1550 cm^{-1} can be assigned to the symmetric and antisymmetric COO^- stretching modes, and stronger intensities for the two peaks were observed from the ACN-washed QD surface compared with MeOH-washed QD surface, indicating that more oleate was bound to the QD surface washed by ACN. In addition, the stronger peaks of I $3d_{5/2}$ and I $3d_{3/2}$ in the I 3d XPS spectra were observed for the ACN-washed QD surface, which indicated that ACN washing could facilitate successful ligand exchange with PbI_2 (see Figure S4 in the Supporting Information). Because it has been proven in the previous reports that Pb−OH is one of the main causes of the sub-band gap trap states in PbS QDs, the minimized −OH content after ACN washing illustrated that our strategy can effectively cure the surface trap states of PbS QDs and reduce the interface charge recombination.[16,18]

3.2. Photovoltaic Performance of PbS QDSCs. To investigate the influence of ACN washing and MeOH washing on the PbS QDs, we fabricated PbS QDSCs with the structure of ITO/SnO_2/n-PbS/p-PbS/Au by using ACN-washed PbS QDs and MeOH-washed PbS QDs, respectively, where the SnO_2 ETL was passivated by $SnCl_2$. The passivation of the SnO_2 ETL showed a suppressed charge combination in the interface of PbS/SnO_2 (see Figure S1 and Table S1 in the Supporting Information), which improved the best PCE of the corresponding solar cells from 7.48 to 8.53% (see Figure S2 and Table S2 in the Supporting Information). More details and corresponding discussion can be obtained from the Supporting Information. The photocurrent−photovoltage characteristics of the champion PbS QDSCs are shown in Figure 3a, and the corresponding photovoltaic performance parameters are listed in Table 1. The results showed that the MeOH-washed PbS

https://doi.org/10.1021/acsomega.4c00208
ACS Omega 2024, 9, 12211−12218

Table 1. Photovoltaic Performance Parameters of PbS QDSCs with Different Precipitants

precipitant	J_{sc} (mA·cm^{-2})	V_{oc} (V)	FF	PCE (%)
ACN	28.26	0.58	0.64	10.49
MeOH	24.19	0.56	0.63	8.53

QDSC had a short-circuit photocurrent density (J_{sc}) of 24.19 mA·cm^{-2}, an open-circuit voltage (V_{oc}) of 0.56 V, and a fill factor (FF) of 0.63. In clear contrast, enhanced J_{sc} of 28.26 mA·cm^{-2}, V_{oc} of 0.58 V, and FF of 0.64 were achieved in the ACN-washed PbS QDSCs, which boosted the PCE from 8.53 to 10.49%. Although the PCE of 10.49% was lower than most ZnO ETL-based PbS QDSCs, it was a high efficiency for SnO_2 ETL-based PbS QDSCs. The distinctly improved photovoltaic performance can be attributed to the minimization of −OH content on the surface of PbS QDs washed by ACN, which effectively decreased the trap states on the surface of PbS QDs, improved the quality of PbS QDs, and enhanced the charge transport in devices. To ensure the reproducibility of the above results, we assembled around 50 devices each for ACN-washed and MeOH-washed PbS QDSCs, and the corresponding PCE distribution is shown in Figure 3b. As shown in Figure 3b, the PCE distribution of MeOH-washed PbS QDSCs was from 6 to 8.5%, whereas an improved PCE distribution of 8 to 10.5% for ACN-washed PbS QDSCs was achieved, demonstrating the reliability of our strategy by using ACN to reduce surface trap states of PbS QDs, which can improve the photovoltaic performance of devices.

Figure 4 summarizes the photovoltaic performance of ACN-washed PbS QDSCs and MeOH-washed PbS QDSCs with different thicknesses of light absorption layer. In agreement with previous reports, the J_{sc}, V_{oc}, and FF of MeOH-washed PbS QDSCs increased with the absorber thickness increased from 250 to 350 nm, and then all decreased dramatically when the absorber thickness continued to increase from 350 to 550 nm, which can be attributed to insufficient carrier diffusion lengths.[12,31−33] For ACN-washed PbS QDSCs, the J_{sc}, V_{oc}, and FF reached the highest level when the absorber thickness reached 450 nm; therefore, the MeOH-washed PbS QDSCs and ACN-washed PbS QDSCs obtained the best PCE for the optimum absorber thickness of 350 and 450 nm, respectively. The result indicated that our strategy of using ACN to treat the surface of PbS QDs played an important role in extending the carrier diffusion lengths and enhancing the carrier transporting in PbS QDSCs, corresponding to the improved photovoltaic performance of ACN-washed PbS QDSCs.

3.3. Effect of ACN-Washed PbS QDs on Surface Trap State Reduction. To confirm the surface trap state reduction of ACN-washed PbS QDs, SCLC measurements were applied on electron-only devices with the structure of ITO/SnO_2/n-PbS/BCP/C_{60}/Ag and hole-only devices with the structure of ITO/PEDOT:PSS/p-PbS/*spiro*-OMeTAD/Au. The n-PbS and p-PbS were obtained via ligand exchange of o-PbS and

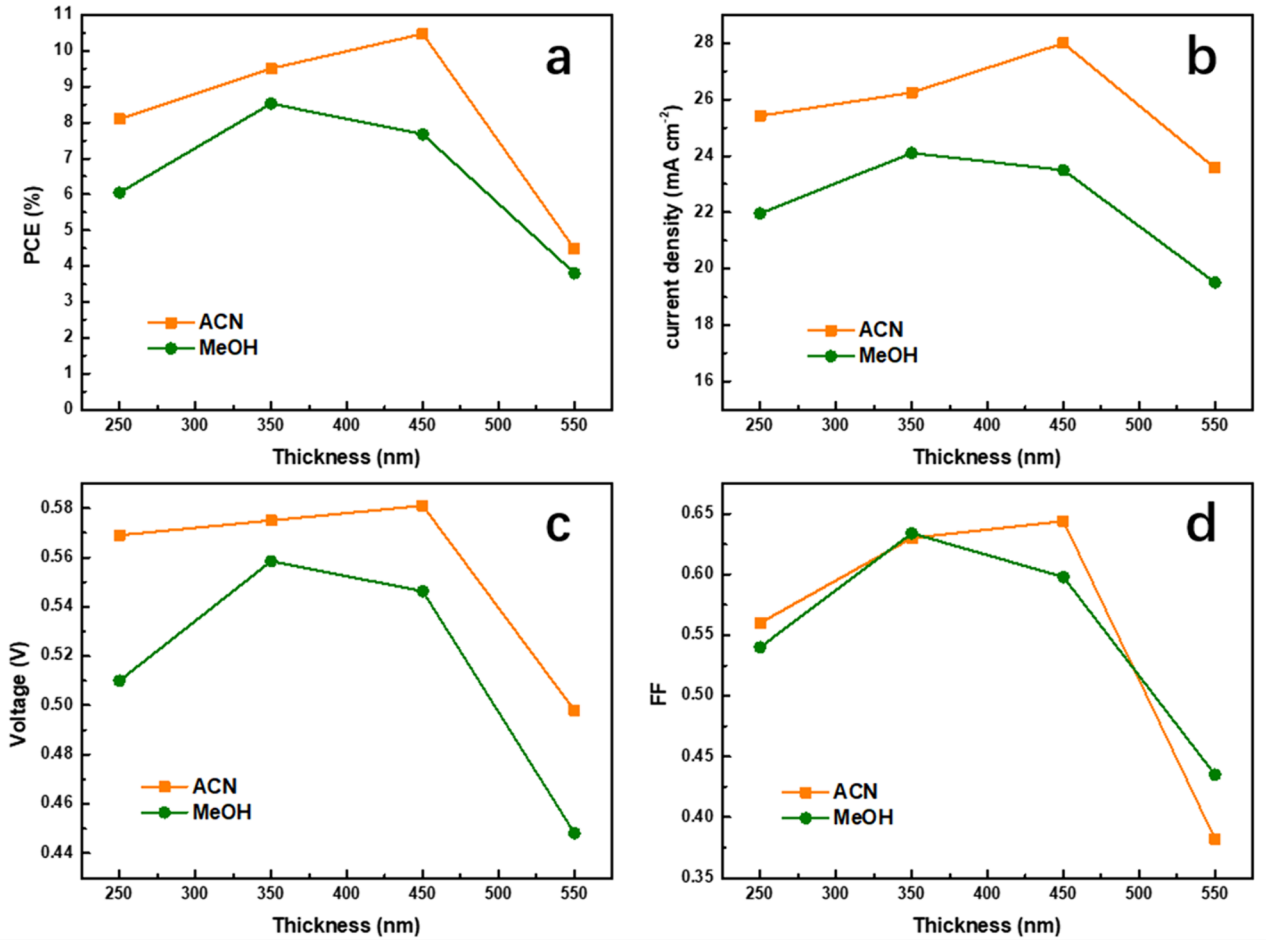

Figure 4. (a) PCE, (b) J_{sc}, (c) V_{oc}, and (d) FF of ACN-washed PbS QDSCs and MeOH-washed PbS QDSCs with different absorber thicknesses.

https://doi.org/10.1021/acsomega.4c00208
ACS Omega 2024, 9, 12211−12218

PbI_2, and o-PbS and EDT, respectively. As shown in Figure 5, a linear (ohmic) increase appeared first at lower voltages, and a

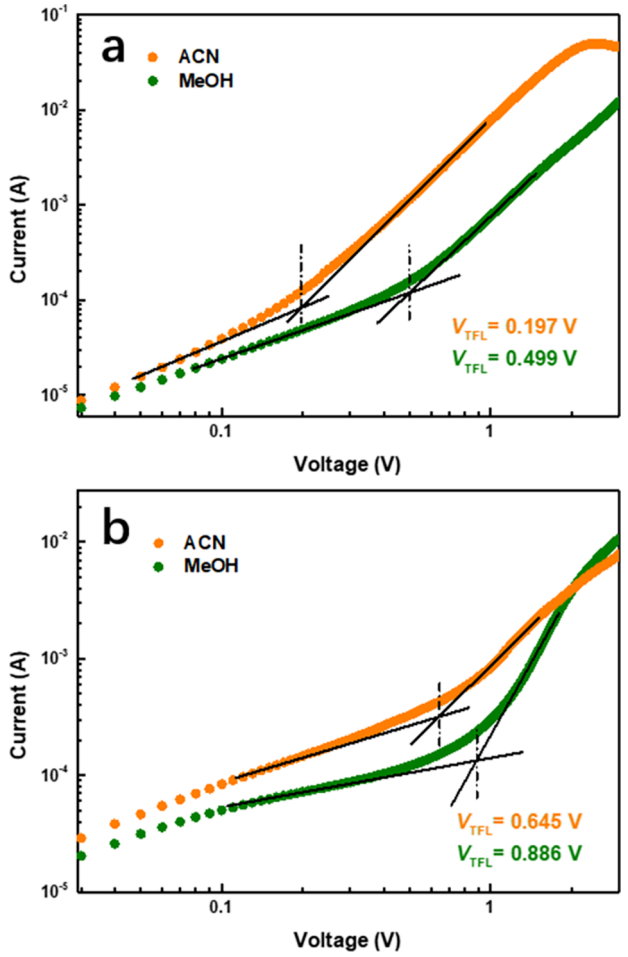

Figure 5. SCLC curves of (a) electron-only devices and (b) hole-only devices based on ACN-washed o-PbS and MeOH-washed o-PbS.

greater logarithmic slope can be observed with the rise of voltages, which represented the trap-filling. Normally, the trap-filling voltage (V_{TFL}) is defined by the voltage corresponding to the intersection of the two lines with the resulting slopes.[26] The V_{TFL}'s of the electron-only devices based on n-PbS films from ACN-washed o-PbS and MeOH-washed o-PbS were 0.197 and 0.499 V, respectively. The V_{TFL}'s of the hole-only devices based on p-PbS films from ACN-washed o-PbS and MeOH-washed o-PbS were 0.645 and 0.886 V, respectively. The trap state density (N_{trap}) can be estimated by V_{TFL} with the following equation[33]:

$$N_{trap} = \frac{2\varepsilon_0 \varepsilon V_{TFL}}{eL^2} \quad (1)$$

where ε_0 was the vacuum permittivity, ε was the relative dielectric constant of PbS (ε = 17.2),[34] e was the electron charge, and L was the film thickness. According to the equation, the electron trap densities of n-PbS films based on ACN-washed o-PbS and MeOH-washed o-PbS were estimated at 1.85 × 10^{15} and 4.69 × 10^{15} cm^{-3}, whereas the hole trap densities of p-PbS films based on ACN-washed o-PbS and MeOH-washed o-PbS were estimated at 6.06 × 10^{15} and 8.33 × 10^{15} cm^{-3}. The calculation results confirmed a lower trap density of ACN-washed devices, leading to the significant increase of J_{sc}, V_{oc}, and FF of the corresponding PbS QDSCs, which demonstrated that our strategy of using ACN to minimize −OH content on PbS QDs surface was an effective way for reducing surface trap states of PbS QDs, improving the quality of PbS films, and achieving high photovoltaic performance of PbS QDSCs. To further understand the relationship of defects and the photovoltaic performance of PbS QDSCs, as shown in Figure 6, the defect density was

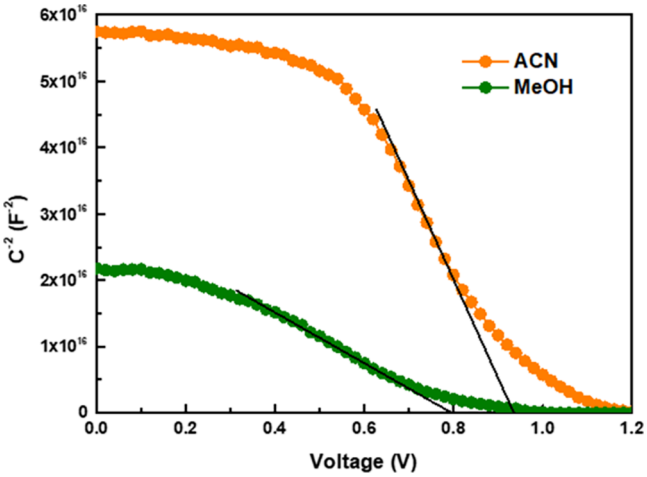

Figure 6. $C-V$ curves of ACN-washed and MeOH-washed PbS QDSCs.

determined by the Mott−Schottky equation using the capacitance−voltage ($C-V$) characterization[35]:

$$N_a = -\frac{2}{q\varepsilon_0 \varepsilon A^2} \times \left[\frac{d}{dV}\left(\frac{1}{C^2}\right)\right]^{-1} \quad (2)$$

where N_a was the defect density, C was the capacitance, and A was the active area of PbS QDSCs. After calculation, the estimated defect density of ACN-washed PbS QDSCs was 8.74 × 10^{15} cm^{-3}, which was only a quarter of that for MeOH-washed PbS QDSCs (3.34 × 10^{16} cm^{-3}). Again, the lower defect density of ACN-washed PbS QDSCs indicated that the ACN-washed PbS QDs were essential for achieving significant trap state reduction and photovoltaic performance improvement.

The influence of the PbS QD trap states on the charge transporting and recombination of PbS QDSCs was investigated by analyzing EIS and light-intensity dependent V_{oc}. First, Figure 7a shows the Nyquist plots of ACN-washed and MeOH-washed PbS QDSCs, and the corresponding fitted data by an equivalent circuit R_s (R_{cr} CPE) are listed in Table 2. R_s was the serial resistance describing the resistance of the ITO and Au electrode, whereas R_{cr} represented the charge recombination resistance on the interface of PbS/SnO_2. The constant phase element (CPE) was a nonideal frequency-dependent capacitance, of which the admittance can be expressed by the following equation:

$$Y_Q = Y_0(j\omega)^n \quad (3)$$

where n was a constant ranging from 0 to 1 that described the difference from the ideal capacitance and Y_0 represented the capacitance of the PbS/SnO_2 interface.[5,36−39] Therefore, the small difference of R_s between ACN-washed and MeOH-washed PbS QDSCs can be attributed to the same ITO

https://doi.org/10.1021/acsomega.4c00208
ACS Omega 2024, 9, 12211−12218

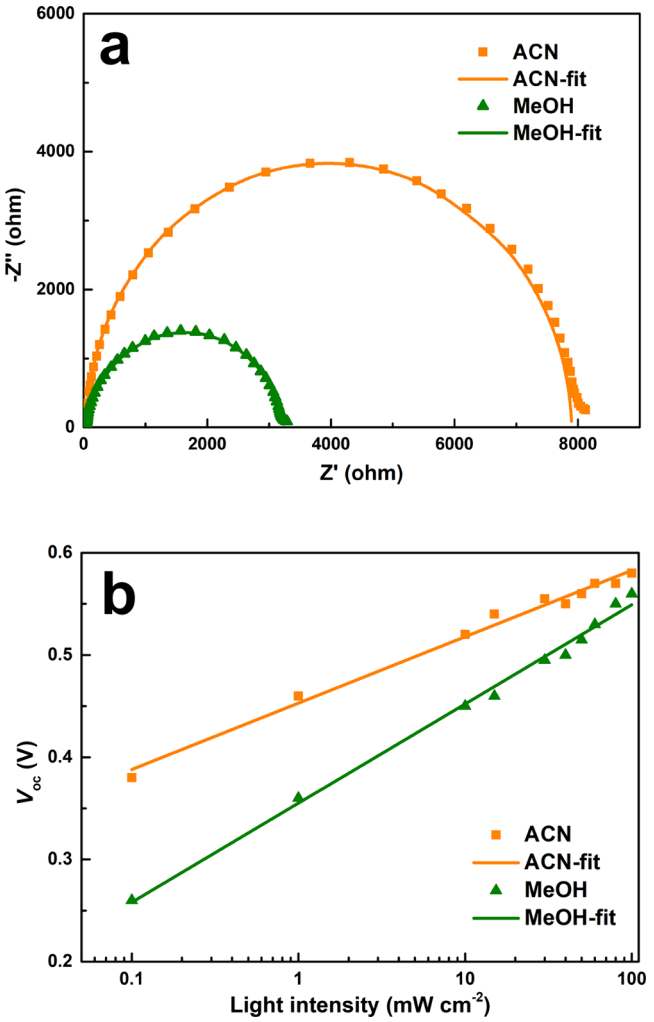

Figure 7. (a) Nyquist plots and (b) light-intensity-dependent V_{oc} for ACN-washed and MeOH-washed PbS QDSCs.

Table 2. Parameters Obtained by Fitting the Experimental Data with the Equivalent Circuit R_s (R_{cr} CPE)

solar cell	R_s (Ω)	R_{cr} (Ω)	Y_0 (10^{-8}·F·s^{n-1})	n
ACN washed	33.89	7862	3.58	0.987
MeOH washed	31.16	3209	10.67	0.906

substrate and electrode material of Au for fabricating PbS QDSCs. On the other hand, higher R_{cr} (7862 Ω) and lower Y_0 (3.58×10^{-8}·F·s^{n-1}) of ACN-washed PbS QDSCs than those of MeOH-washed PbS QDSCs (3209 Ω and 10.67×10^{-8}·F·s^{n-1}, respectively) were obtained. The result indicated that the charge recombination at the interface of SnO_2/PbS was suppressed by using ACN-washed PbS QDs, leading to improved interface charge separation and transport, which was consistent with the obviously enhanced photovoltaic performance of ACN-washed PbS QDSCs. As shown in Figure 7b, the light-intensity dependent V_{oc} can be determined by the following equation[29]:

$$V_{oc} = \frac{nkT}{q}\alpha \ln I + C \quad (4)$$

where n was the diode ideality factor, k was the Boltzmann constant, T was the temperature, q was the elementary charge, α was the exponential factor, I was the light intensity, and C was the fitting parameter. The slopes of ACN-washed and MeOH-washed PbS QDSCs were $1.08kT/q$ and $1.62kT/q$, respectively, demonstrating that the trap-assisted charge recombination was effectively suppressed by ACN washing. The result was in accordance with reduced trap density and improved V_{oc} and FF values of ACN-washed PbS QDSCs.

3.4. Stability of PbS QDSCs. The stability test of PbS QDSCs was also an important way to evaluate the surface condition of PbS QDs and the quality of the PbS QDSCs.[29,30] Therefore, the PCE evolutions in a long storage time of ACN-washed and MeOH-washed PbS QDSCs without encapsulation were tested in a nitrogen atmosphere and in ambient air with a relative humidity of around 60%, respectively. As shown in Figure 8a, for the storage in nitrogen atmosphere, both the

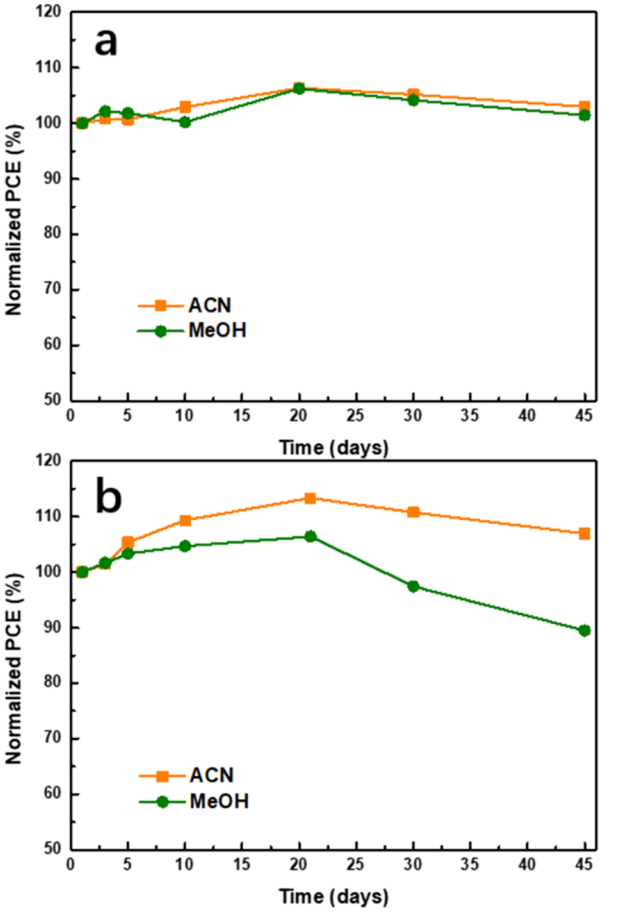

Figure 8. Long-term stability under (a) a nitrogen atmosphere and (b) ambient air of unencapsulated ACN-washed and MeOH-washed PbS QDSCs.

ACN-washed and MeOH-washed PbS QDSCs showed good stability with no significant decays of PCE for 45 days. However, from Figure 8b, for storage in ambient air, the MeOH-washed PbS QDSCs retained only about 90% of their original PCE after 45 days, wheresa the ACN-washed PbS QDSCs can still maintain over 105% of their original PCE after 45 days with a much slower trend of efficiency decay, possessing a better long-term air stability. The result demonstrated the improved surface condition of ACN-washed PbS QDs, which was in good agreement with the enhanced photovoltaic performance of ACN-washed PbS QDSCs.[29]

https://doi.org/10.1021/acsomega.4c00208
ACS Omega 2024, 9, 12211−12218

4. CONCLUSIONS

In summary, we developed an effective strategy to prepare high-quality PbS QDs with reduced surface trap states by using ACN as a precipitant to wash the surface of PbS QDs. The use of ACN can minimize the surface −OH content of PbS QDs, leading to reduced surface trap states of PbS QDs. The PbS QDSCs based on ACN-washed PbS QDs with the structure of ITO/SnO_2/n-PbS/p-PbS/Au were successfully fabricated, which achieved a high PCE of 10.49% with enhanced air storage stability for SnO_2 ETL-based PbS QDSCs. It may be anticipated that our strategy will expand the way that high-quality QDs and efficient photovoltaic devices are fabricated in future studies.

■ ASSOCIATED CONTENT

Supporting Information

The Supporting Information is available free of charge at https://pubs.acs.org/doi/10.1021/acsomega.4c00208.

The following files are available free of charge. Photovoltaic performance parameters of PbS QDSCs with SnO_2 and passivited- SnO_2 ETL, EIS analysis of PbS QDSCs with SnO_2 ETL and passivated-SnO_2 ETL, Photos of o-PbS standing for 20 s after adding MeOH and ACN, TEM image of PbS QDs after ACN washing, I 3d XPS spectra of ACN-washed and MeOH-washed PbS QDs after ligand exchange with PbI_2 (PDF)

■ AUTHOR INFORMATION

Corresponding Authors

Guannan Xiao − *Chengdu Polytechnic, Chengdu 610041, P. R. China; Material Corrosion and Protection Key Laboratory of Sichuan Province, Zigong 643002, P. R. China;* orcid.org/0009-0009-8364-3848; Email: shaw_gn@163.com, xiaoguannan@cdp.edu.cn

Chengwu Shi − *School of Chemistry and Chemical Engineering, Hefei University of Technology, Hefei 230009, P. R. China;* orcid.org/0000-0001-5112-1425; Email: shicw506@foxmail.com, shicw506@hfut.edu.cn

Authors

Taohua Liang − *Chengdu Polytechnic, Chengdu 610041, P. R. China*

Xiaoming Wang − *Chengdu Polytechnic, Chengdu 610041, P. R. China*

Chao Ying − *School of Chemistry and Materials Engineering, Anhui Key Laboratory of Low Temperature Co-fired Materials, Huainan Normal University, Huainan 232038, P. R. China*

Kai Lv − *School of Chemistry and Chemical Engineering, Hefei University of Technology, Hefei 230009, P. R. China*

Complete contact information is available at: https://pubs.acs.org/10.1021/acsomega.4c00208

Author Contributions

The manuscript was written through contributions of all authors. All authors have given approval to the final version of the manuscript.

Notes

The authors declare no competing financial interest.

■ ACKNOWLEDGMENTS

This work was financially supported by the National Natural Science Foundation of China (51972091), the Sichuan Provincial Natural Science Foundation Youth Fund Project (2023NSFSC1178), the Opening Project of Material Corrosion and Protection Key Laboratory of Sichuan province (2023CL08), the Key Scientific Research Projects of Colleges and Universities in Anhui Province (2023AH051541), the Research and Development Centre of Photovoltaic Technology with Renewable Energy (23KYPT03), and the Scientific Research Projects of Chengdu Polytechnic (23CZYG046).

■ REFERENCES

(1) Saran, R.; Curry, R. J. Lead sulphide nanocrystal photodetector technologies. *Nat. Photonics* **2016**, *10*, 81−92.

(2) Carey, G. H.; Abdelhady, A. L.; Ning, Z.; Thon, S. M.; Bakr, O. M.; Sargent, E. H. Colloidal quantum dot solar cells. *Chem. Rev.* **2015**, *115*, 12732−12763.

(3) Kagan, C. R.; Murray, C. B. Charge transport in strongly coupled quantum dot solids. *Nat. Nanotechnol.* **2015**, *10*, 1013−1026.

(4) Kim, S.; Kim, J.; Lee, Y. H. Carrier multiplication in PbS quantum dots anchored on a Au tip using conductive atomic force microscopy. *Adv. Mater.* **2020**, *32*, No. 1908461.

(5) Sun, L.; Choi, J. J.; Stachnik, D.; Bartnik, A. C.; Hyun, B.-R.; Malliaras, G. G.; et al. Bright infrared quantum-dot light-emitting diodes through inter-dot spacing control. *Nat. Nanotechnol.* **2012**, *7*, 369−373.

(6) Konstantatos, G.; Howard, I.; Fischer, A.; Hoogland, S.; Clifford, J.; Klem, E.; et al. Ultrasensitive solution-cast quantum dot photodetectors. *Nature* **2006**, *442*, 180−183.

(7) Chuang, C. H. M.; Brown, P. R.; Bulovic, V.; Bawendi, M. G. Improved performance and stability in quantum dot solar cells through band alignment engineering. *Nat. Mater.* **2014**, *13*, 796−801.

(8) Hines, M. A.; Scholes, G. D. Colloidal PbS nanocrystals with size-tunable near-infrared emission: Observation of post-synthesis self-narrowing of the particle size distribution. *Adv. Mater.* **2003**, *15*, 1844−1849.

(9) Kroupa, D. M.; Vörös, M.; Brawand, N. P.; McNichols, B. W.; Miller, E. M.; Gu, J.; Nozik, A. J.; Sellinger, A.; Galli, G.; Beard, M. C.; et al. Tuning colloidal quantum dot band edge positions through solution-phase surface chemistry modification. *Nat. Commun.* **2017**, *8*, 15257.

(10) Tang, J.; Kemp, K. W.; Hoogland, S.; Jeong, K. S.; Liu, H.; Levina, L.; et al. Colloidal-quantum-dot photovoltaics using atomic-ligand passivation. *Nat. Mater.* **2011**, *10*, 765−771.

(11) Liu, M.; Voznyy, O.; Sabatini, R.; García de Arquer, F. P.; Munir, R.; Balawi, A. H.; et al. Hybrid organic-inorganic inks flatten the energy landscape in colloidal quantum dot solids. *Nat. Mater.* **2017**, *16*, 258−263.

(12) Ning, Z.; Voznyy, O.; Pan, J.; Hoogland, S.; Adinolfi, V.; Xu, J.; et al. Air-stable n-type colloidal quantum dot solids. *Nat. Mater.* **2014**, *13*, 822−828.

(13) Wang, W.; Zhao, L.; Wang, Y.; Xue, W.; He, F.; Xie, Y.; Li, Y. A facile secondary deposition for improving quantum dot loading in fabricating quantum dot solar cells. *J. Am. Chem. Soc.* **2019**, *141*, 4300−4307.

(14) Wang, W.; Feng, W.; Du, J.; Xue, W.; Zhang, L.; Zhao, L.; Li, Y.; Zhong, X. Cosensitized quantum dot solar cells with conversion efficiency over 12%. *Adv. Mater.* **2018**, *30* (2018), No. 1705746.

(15) Choi, M. J.; García de Arquer, F. P.; Proppe, A. H.; Seifitokaldani, A.; Choi, J.; Kim, J.; Baek, S. W.; Liu, M.; Sun, B.; Biondi, M.; Scheffel, B.; Walters, G.; Nam, D. H.; Jo, J. W.; Ouellette, O.; Voznyy, O.; Hoogland, S.; Kelley, S. O.; Jung, Y. S.; Sargent, E. H.; et al. Cascade surface modification of colloidal quantum dot inks enables efficient bulk homojunction photovoltaics. *Nat. Commun.* **2020**, *11*, 103.

(16) Zherebetskyy, D.; Scheele, M.; Zhang, Y. J.; Bronstein, N.; Thompson, C.; Britt, D.; et al. Hydroxylation of the surface of PbS nanocrystals passivated with oleic acid. *Science* **2014**, *344*, 1380−1384.
(17) Azmi, R.; Sinaga, S.; Aqoma, H.; Seo, G.; Ahn, T. K.; Park, M.; et al. Highly efficient air-stable colloidal quantum dot solar cells by improved surface trap passivation. *Nano Energy* **2017**, *39*, 86−94.
(18) Cao, Y.; Stavrinadis, A.; Lasanta, T.; So, D.; Konstantatos, G. The role of surface passivation for efficient and photostable PbS quantum dot solar cells. *Nat. Energy* **2016**, *1*, 16035.
(19) Hendry, E.; Koeberg, M.; O'Regan, B.; Bonn, M. Local field effects on electron transport in nanostructured TiO_2 revealed by Terahertz spectroscopy. *Nano Lett.* **2006**, *6*, 755−759.
(20) Arnold, M. S.; Avouris, P.; Pan, Z. W.; Wang, Z. L. Field-effect transistors based on single semiconducting oxide nanobelts. *J. Phys. Chem. B* **2003**, *107*, 59−663.
(21) Seager, C. H.; Myers, S. M. Quantitative comparisons of dissolved hydrogen density and the electrical and optical properties of ZnO. *J. Appl. Phys.* **2003**, *94*, 2888.
(22) Tiwana, P.; Docampo, P.; Johnston, M. B.; Snaith, H. J.; Herz, L. M. Electron mobility and injection dynamics in mesoporous ZnO, SnO_2, and TiO_2 Films used in dye-sensitized solar cells. *ACS Nano* **2011**, *5*, 5158−5166.
(23) Khan, J.; Yang, X.; Qiao, K.; Deng, H.; Zhang, J.; Liu, Z.; et al. Low-temperature-processed SnO2-Cl for efficient PbS quantum-dot solar cells via defect passivation. *J. Mater. Chem. A* **2017**, *5*, 17240−17247.
(24) Li, Y.; Yang, F.; Wang, Y.; Shi, G.; Maung, Y. M.; Yuan, J.; Huang, S.; Ma, W.; et al. Magnetron Sputtered SnO_2 Constituting Double Electron Transport Layers for Efficient PbS Quantum Dot Solar Cells. *Sol. RRL* **2020**, *4*, No. 2000218.
(25) Barkhouse, D. A. R.; Debnath, R.; Kramer, I. J.; Zhitomirsky, D.; Pattantyus-Abraham, A. G.; Levina, L.; et al. Depleted bulk heterojunction colloidal quantum dot photovoltaics. *Adv. Mater.* **2011**, *23*, 3134−3138.
(26) Hao, M.; Bai, Y.; Zeiske, S.; Ren, L.; Liu, J.; Yuan, Y.; Zarrabi, N.; Cheng, N.; Ghasemi, M.; Chen, P.; Lyu, M.; He, D.; Yun, J. H.; Du, Y.; Wang, Y.; Ding, S.; Armin, A.; Meredith, P.; Liu, G.; Cheng, H. M.; Wang, L.; et al. Ligand-assisted cation-exchange engineering for high-efficiency colloidal $Cs_{1-x}FA_xPbI_3$ quantum dot solar cells with reduced phase segregation. *Nat. Energy* **2020**, *5*, 1−10.
(27) Guo, Z.; Teo, S.; Xu, Z.; Zhang, C.; Kamata, Y.; Hayase, S.; et al. Achievable high Voc of carbon based all-inorganic $CsPbIBr_2$ perovskite solar cells through interface engineering. *J. Mater. Chem. A* **2019**, *7*, 1227−1232.
(28) Shi, D.; Adinolfi, V.; Comin, R.; Yuan, M.; Alarousu, E.; Buin, A.; et al. Low trap-state density and long carrier diffusion in organolead trihalide perovskite single crystals. *Science* **2015**, *347*, 519−522.
(29) Gu, M.; Wang, Y.; Yang, F.; Lu, K.; Xue, Y.; Wu, T.; Fang, H.; Zhou, S.; Zhang, Y.; Ling, X.; Xu, Y.; Li, F.; Yuan, J.; Loi, M. A.; Liu, Z.; Ma, W. Stable PbS quantum dot ink for efficient solar cells by solution-phase ligand engineering. *J. Mater. Chem. A* **2019**, *7*, 15951−15959.
(30) Wang, Y.; Lu, K.; Han, L.; Liu, Z.; Shi, G.; Fang, H.; Chen, S.; Wu, T.; Yang, F.; Gu, M.; Zhou, S.; Ling, X.; Tang, X.; Zheng, J.; Loi, M. A.; Ma, W.; et al. In situ passivation for efficient PbS quantum dot solar cells by precursor engineering. *Adv. Mater.* **2018**, *30*, No. 1704871.
(31) Xu, J.; Voznyy, O.; Liu, M.; Kirmani, A. R.; Walters, G.; Munir, R.; et al. 2D matrix engineering for homogeneous quantum dot coupling in photovoltaic solids. *Nat. Nanotechnol.* **2018**, *13*, 456−462.
(32) Lan, X.; Voznyy, O.; García de Arquer, F. P.; Liu, M.; Xu, J.; Proppe, A. H.; et al. 10.6% certified colloidal quantum dot solar cells via solvent-polarity-engineered halide passivation. *Nano Lett.* **2016**, *16*, 4630−4634.
(33) Chen, P.; Wang, Z.; Wang, S.; Lyu, M.; Hao, M.; Ghasemi, M.; et al. Luminescent europium-doped titania for efficiency and UV-stability enhancement of planar perovskite solar cells. *Nano Energy* **2020**, *69*, No. 104392.
(34) Brown, P. R.; Kim, D.; Lunt, R. R.; Zhao, N.; Bawendi, M. G.; Grossman, J. C.; et al. Energy level modification in lead sulfide quantum dot thin films through ligand exchange. *ACS Nano* **2014**, *8*, 5863−5872.
(35) Liu, X.; Wu, T.; Chen, J.-Y.; Meng, X.; He, X.; Noda, T.; et al. Templated growth of $FASnI_3$ crystals for efficient tin perovskite solar cell. *Energy Environ. Sci.* **2020**, *13*, 2896−2902.
(36) Liu, C.; Qiu, Z.; Meng, W.; Chen, J.; Qi, J.; Dong, C.; et al. Effects of interfacial characteristics on photovoltaic performance in $CH_3NH_3PbBr_3$-based bulk perovskite solar cells with core/shell nanoarray as electron transporter. *Nano Energy* **2015**, *12*, 59−68.
(37) Mora-Sero, I.; Bisquert, J.; Fabregat-Santiago, F.; Garcia-Belmonte, G.; Zoppi, G.; Durose, K.; et al. Implications of the negative capacitance observed at forward bias in nanocomposite and polycrystalline solar cells. *Nano Lett.* **2006**, *6*, 640−650.
(38) Ma, J.; Yang, G.; Qin, M.; Zheng, X.; Lei, H.; Chen, C.; Chen, Z.; Guo, Y.; Han, H.; Zhao, X.; Fang, G.; et al. MgO nanoparticle modified anode for highly efficient SnO_2-based planar perovskite solar cells. *Adv. Sci.* **2017**, *4*, No. 1700031.
(39) Xiao, G.; Shi, C.; Lv, K.; Ying, C.; Wang, Y. Nb-doping TiO_2 electron transporting layer for efficient perovskite solar cells. *ACS Appl. Energy Mater.* **2018**, *1*, 2576−2581.

https://doi.org/10.1021/acsomega.4c00208
ACS Omega 2024, 9, 12211−12218